Modelling of volcanic ash with HYSPLIT and satellite observations: a case study of the 2018 Barren Island volcano eruption event, Andaman Territory, India

Goutham Krishna Teja Gunda[1,*], P. K. Champatiray[1], Mamta Chauhan[1], Prakash Chauhan[1], Mijanur Ansary[1], Arya Singh[1], Yateesh Ketholia[1] and S. Balaji[2]

[1]Geosciences and Disaster Management Studies Group, Indian Institute of Remote Sensing (ISRO), Dehradun 248 001, India
[2]Department of Disaster Management, Pondicherry University, Port Blair 744 101, India

The present study aims to identify, characterize monitor and model the transport pathways of volcanic ashes and various features of the active phase of Barren Island volcano (BIV), Andaman and Nicobar Island, India during 2018 using the several Earth observation satellite technologies and field observations in the study area. Sentinel-2 satellite datasets have been used to identify volcanic eruption features such as lava flow, ash plume, cinder and vent and different directions of lava flow from the cinder cone during the 2018 eruptive phase of BIV. To visualize the major variations in thermal intensity and understand the behaviour of current volcanic activity, volcanic radiative power (VRP) and radiant fluxes of the recent eruptive phase were calculated using MIROVA. In addition, thermal anomaly was observed in the form of anomalous fire pixels for 44 days in FIRMS database. Also, NASA/NOAA Visible Infrared Imaging Radiometer Suite (VIIRS, VNP14IMGT) were used for validating the real-time activity of the 2018 volcanic eruption phase. The results obtained were closely related with the periods of high eruptions as observed in the Sentinel-2 datasets. The volcanic aerosol 'sulphur dioxide' (SO_2) data (time series-area averaged) were analysed as well as a five-day forward trajectory and volcanic ash model for each eruption event was developed using HYSPLIT model to identify the transport pathways and extent of volcanic ash cloud in the lower atmosphere during the eruptive phase of the volcano.

Keywords: Eruptive phase, field observations, satellite observations, volcanic ash.

BARREN Island volcano (BIV), the young and only confirmed active volcano of South Asia lies in the north-eastern Indian Ocean, i.e. in the Andaman Sea within the Indian territory. It is located ~138 km NE of Port Blair, the capital of the Andaman and Nicobar Islands and within an active subduction zone (Figure 1). BIV is an uninhabited strato-volcano with an elevation of ~350 m amsl. The currently exposed region is just the upper part of the volcano, whereas almost 90% of the volcano is submerged in water as revealed by recent bathymetry data. It consists of the caldera, which is breached towards the west by alternating lava flows and volcanic deposits, with polygenetic vent at the centre[1,2] (Figure 1). This volcanic island is the resultant of several pre-historic (unknown years) and historical eruptions reported between 1787 and 1832 with sporadic eruptions in 1991, 1995, 2005–2007, 2008–2010, 2013–2016 and 2017 and at present (https://volcano.si.edu/volcano.Cfm?vn=260010). This volcano began its active phase of eruption in 1991 and now it is in a 'strombolian activity' type of eruption with low- to moderate-scale ash and lava eruptions from either its central polygenetic vent or secondary vents located at its flanks[1]. The current eruption of BIV is considered to be protraction of the recent eruptive phase that began in 2005 intermittently spewing lava, pyroclastic materials and ashes[2]. Since 2005, it has become active, particularly during active seismic periods around the intersection point of the West Andaman Fault (WAF) and Sunda Fault System (SFS). Recently, BIV has started emitting lava and plumes since 25 September 2018.

In recent decades, the acquisition of satellite images and datasets for volcano-related studies has increased rapidly throughout the globe[3–5]. Moreover, remote sensing technology has played a key role in monitoring and characterizing active volcanoes around the world[3,6] mainly for real-time monitoring of eruptions[7], especially in the case of remote and inaccessible areas of active volcanoes. With the availability of several high-resolution data, the possibility has increased, especially in the case of recognized active volcanoes, which are well known for their violent behaviour. Many researchers have utilized

*For correspondence. (e-mail: krishna.g366@gmail.com)

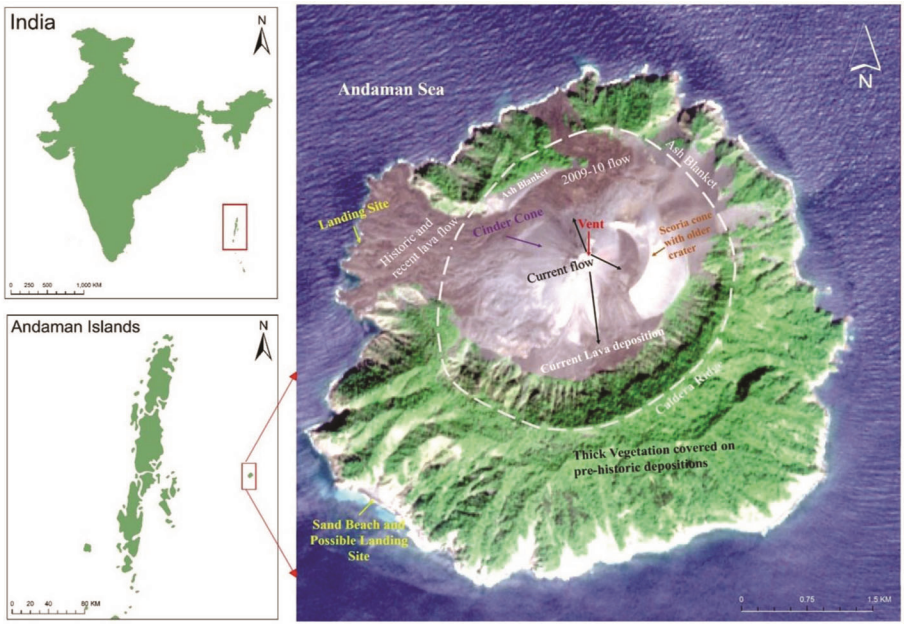

Figure 1. A simplified map of Barren Island volcano (BIV) Andaman and Nicobar (A&N) Islands overlaid on Sentinel-2 satellite image (acquired on 22 November 2018) (RGB-4 : 3 : 2). Some significant morphological features of the volcano are highlighted.

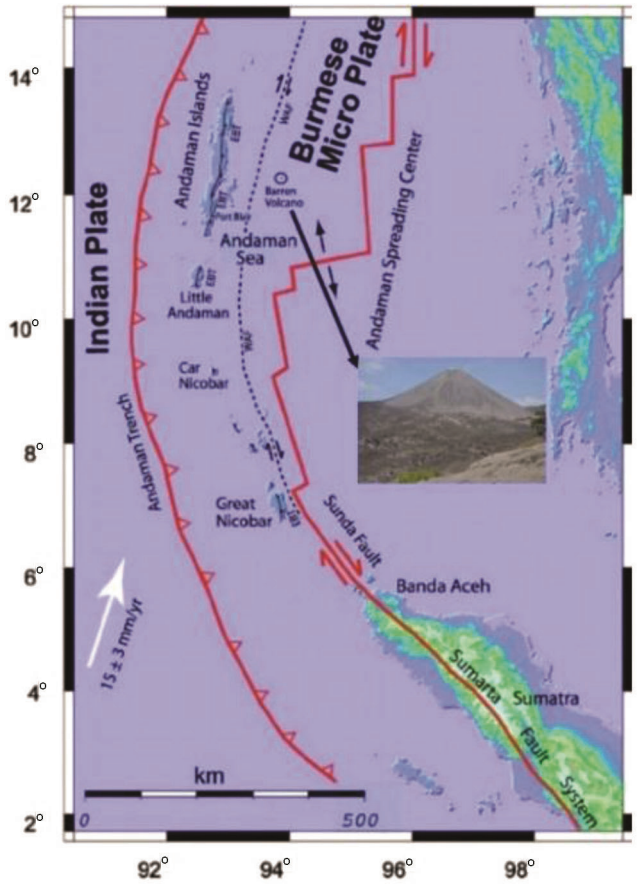

Figure 2. Location of Barren Island and geological setting of A&N Islands (modified after Malik 2005) showing complex tectonic regime with compression (subduction), expansion and strike–slip movement along the Sunda Fault (Sumatra Fault System).

various high-resolution satellite data for continuous monitoring of such violent volcanoes throughout the world. For example: Moderate Resolution Imaging Spectroradiometer (MODIS)[8–11], Advanced Space borne Thermal Emission and Reflection Radiometer (ASTER)[12], Landsat series[13,14] and SENTINEL series[15,16]. Therefore, the possibility of continuous monitoring and understanding the natural mechanism has increased, which is crucial to predict and forecast future eruptions and improve the long-term forecasting. It has become more important, especially in the case of recognized active volcanoes which are well known for their violent behaviour. In India, volcanic activities of BIV have been reported using various remote sensing data[7,17–19]. In the present study, we have focused on the 2018 BIV eruption phase with various earth observation satellites along with field observations to identify, characterize, monitor and model the transport pathways of volcanic ashes and volcanic features.

Geological and tectonic setting of the Barren Island

The Barren Island is part of the Neogene Inner Volcanic Arc (NIVA)[20,21] which extends from Mt Popa and Mt Wuntho (extinct volcanoes) in Myanmar in the north to Sumatra and Java in the southeast and intersects at the Pacific Ring of Fire (Figure 2). Moreover, the volcanic arc consists of two exposed volcanoes, viz. Barren Island and Narcondam Island, an active and extinct volcano respectively, along with 22 prominent submarine seamounts enclosed by numerous minor seamounts with

Table 1. Datasets used in the present study

Earth observation satellite	Sensors/bands	Pixel resolution (m)	Date of acquisition	Source
Resourcesat-2	LISS-IV	5.8	12 September 2018	NRSC
Sentinel-2	SWIR-1 and 2	20	13 September 2018 28 September 2018 3 October 2018 18 October 2018 28 October 2018 2 November 2018 7 November 2018	Copernicus Open Access Hub
Volcanic radiative power	MODIS, MIR and thermal bands	50 × 50 km (resampled)	26 September 2018 to 6 November 2018	NASA
HYSPLIT	Volcano trajectories modelling software	–	28 September 2018 3 October 2018 18 October 2018 28 October 2018 2 November 2018	NOAA
Sulphur dioxide	OMI	13 × 24 km	2018	NASA

variable heights and diameters[22]. Barren Island is located just east of the NNW–SSE trending WAF[23], which extends more than 1000 km and joins SFS at Great Nicobar in the Sunda subduction zone[24,25]. The north–south trending WAF is mostly sedentary in the northern part and predominantly strike–slip at the centre and southern segment. Besides, the southern segment has both strike–slip and thrust fault components that generate earthquake swarms mainly at the confluence point of WAF and spreading zones south of 8°N lat. and 94.5°E long.[26,27]. BIV produced basalt and basaltic andesite tephra and lava flows during its active phase from 1787 to 1832 (ref. 2). Interestingly, 'a' ā flows along with tephra were produced during the historical and recent eruption phases which filled the caldera, also called 'caldera-filling 'a' ā flows' that reached the sea through breached western caldera wall during the 1991 eruption[19].

Data and methods

Table 1 provides the details about data products used during this study.

Satellite data

Sentinel-2 is a satellite of the European Space Agency mission developed under the Copernicus programmes and consists of two platforms, i.e. 2A and 2B, launched in June 2015 and March 2017 respectively. On-board instruments capture multispectral images with 13 spectral bands from the visible to shortwave infrared (SWIR) region (viz. 443–2190 nm), with spatial resolution varying from 10 to 60 m. Sentinel-2 revisits every five days at the equator and 2–3 days at mid latitudes. In the present study, we utilized the SWIR (SWIR1–1.610 μm, SWIR2–2.190 μm) band with 20 m spatial resolution, and blue (0.490 μm), green (0.560 μm), red (0.665 μm) and near infrared (NIR, 0.842 μm) bands with 10 m spatial resolution available for cloud-free dates of the year 2018 eruptive phase, which are preferable for continuous monitoring of active volcanoes throughout the world. The Sentinel-2 satellite datasets were obtained for the 2018 eruptive phase (September to November) from Copernicus Open Access Hub (https://scihub.copernicus.eu/dhus/ #/home), which is available for free downloads. The generation of personal geodatabase, preprocessing, processing (involving various bands combinations) and demarcating the latest activities of BIV were carried out using the Arc GIS 10.1 program to identify and demarcate various latest volcanic landforms/features formed in the vicinity of BIV.

Volcanic radiative power

The volcanic radiative power (VRP) was obtained from middle infrared observations of volcanic activity (MIROVA) for detecting thermal anomalies of the Barren Island at high temperatures (>500 K). VRP is used to measure the heat that is radiated by volcanic activity at the time of satellite data acquisition[11]. These datasets are based on the analysis of MODIS (level 1b – calibrated radiances) and automatically processed through MIROVA algorithm[9]. The MODIS moderate spatial and high frequent temporal resolution (four images per day at equatorial latitudes) amalgamate with the middle infrared (MIR) wavelengths, making this sensor dependable for ceaseless monitoring of volcanic activity at the global scale[9,28,29]. MIROVA utilizes two bands, i.e. MIR and thermal TIR at 3.959 and 12.02 μm wavelengths respectively, to calculate different spectral indices such as

normalized thermal index (NTI)[30] and enhanced thermal index (ETI)[9] that improve the incidence of hot objects inside the pixels which helps detect, locate and quantify thermal anomalies at the area of interest. After identifying the pixels, VRP (W) was calculated using Wooster's MIR method[31].

$$VRP = 18.9 \times APIX \times DLMIR,$$

where 18.9 is a best fit regression coefficient (see ref. 31), APIX is the pixel size (1 sq. km for the MODIS pixels) and DLMIR is the 'above background' MIR radiance of the pixel.

In the present study, we acquired VRP time-series data from 26 September 2018 to 6 November 2018, to identify the heat fluxes of BIV and also correlate them with processed observed earth observatory data and derived fire information for resources management system (FIRMS) data.

FIRMS and sulphur dioxide

In addition to VRP, we have acquired FIRMS, which was developed for providing near real time active fire data with three hours of satellite observations from NASA's Visible Infrared Imaging Radiometer Suite (VIIRS) on-board the Suomi National Polar orbiting Partnership (Suomi NPP) and NOAA-20 satellites and MODIS on-board the Terra and Aqua satellites. We acquired the NASA/NOAA Visible Infrared Imaging Radiometer Suite (VIIRS, VNP14IMGT)-based active fire products at 375 m resolution (available at FIRMS, https://firms.modaps.eosdis.nasa.gov/) for validating real-time activity of the 2018 eruption phase, and further correlated with VRP values and observations made from Sentinel-2 datasets.

The sulphur-rich gases (mostly sulphur dioxide (SO_2) gas) are considered as harmful and hazardous, emitted from major explosive volcanic eruptions. The volcanic aerosol 'sulphur dioxide' data (time-series area averaged) were acquired from the Aura OMI (ozone monitoring instrument), which is a contribution of the Netherlands's Agency for Aerospace Programmes (NIVR) in collaboration with the Finnish Meteorological Institute (FMI) to the EOS Aura Mission through the Giovanni NASA website (https://giovanni.gsfc.nasa.ov/giovanni/) for 2018. These data were acquired from the EOS Aura Mission. The data were systemically selected, processed and plotted using the Origin-8 software.

HYSPLIT model analysis

The hybrid single particle Lagrangian integrated trajectory (HYSPLIT) is a Lagrangian transport and dispersion model[32–34] used for modelling the transport and dispersion of volcanic ash[35,36]. This model was developed by the National Oceanic and Atmospheric Administration's Air Resources Laboratory (NOAA ARL; https://www.ready.noaa.gov/HYS PLIT_traj.php) and is operational at the Volcanic Ash Advisory Centers (VAACs), Darwin, Australia. The HYSPLIT model is widely applied in atmospheric pollutant modelling[37,38], as documented by Stein *et al.*[32]. Pertinent to the present study, the HYSPLIT model has been vastly utilized throughout the globe for predicting the transportation of volcanic ash particles in the atmosphere[39,40]. In this study, we have used HYSPLIT trajectories to identify the transport pathways and extent of volcanic ash materials during the 2018 eruption.

Results and discussion

Sentinel-2 datasets

False colour composites (FCC) with different band combinations of Sentinel-2 datasets have been used to identify volcanic features/landforms of BIV, such as lava flow, ash plume, cinder and vent (Figure 3). Further, Sentinel-2 data have been used to identify three different directions of lava flow from the cinder cone. On 28 September 2018, volcanic eruption were observed clearly on the day of the earthquake and the lava flow was observed in the south–southeast direction. It was reported that the actual eruptions of BIV started a couple of days before 28 September 2018, i.e. on 25 September 2018 (https://volcano.si.edu/volcano.cfm?vn=260010). On 3 October 2018, the lava flow direction was towards northwest and east, whereas on 18 October 2018, it has completely changed towards south–southwest direction. On 28 October 2018, the lava flow direction was towards northwest and southeast, whereas on 2 November 2018, no lava flow was observed, but only glowing vent was visible as seen in the satellite data. On 7 November 2018, the vent was not glowing as observed earlier, hence it is interpreted that the phase of volcanic eruption that started on 25 September 2018 continued till 2 November 2018 and finally subsided by 7 November 2018.

Volcanic radiative power

Figure 4 presents the radiant fluxes of the recent eruptive phase of BIV during 2018 (from 26 September 2018 to 6 November 2018, ~42 days), calculated using MIROVA. The displayed VRP time series allowed us to visualize major variations in thermal intensity, to better understand the behaviour of the current volcanic activity. The calculated VRP values were displayed in a megawatt scale, ranging from 1.11 (minimum) to 228.88 MW (maximum), with an overall average of 67.30 MW throughout the selected period. It can be observed from the figure that there is continuous increase in heat flux during the

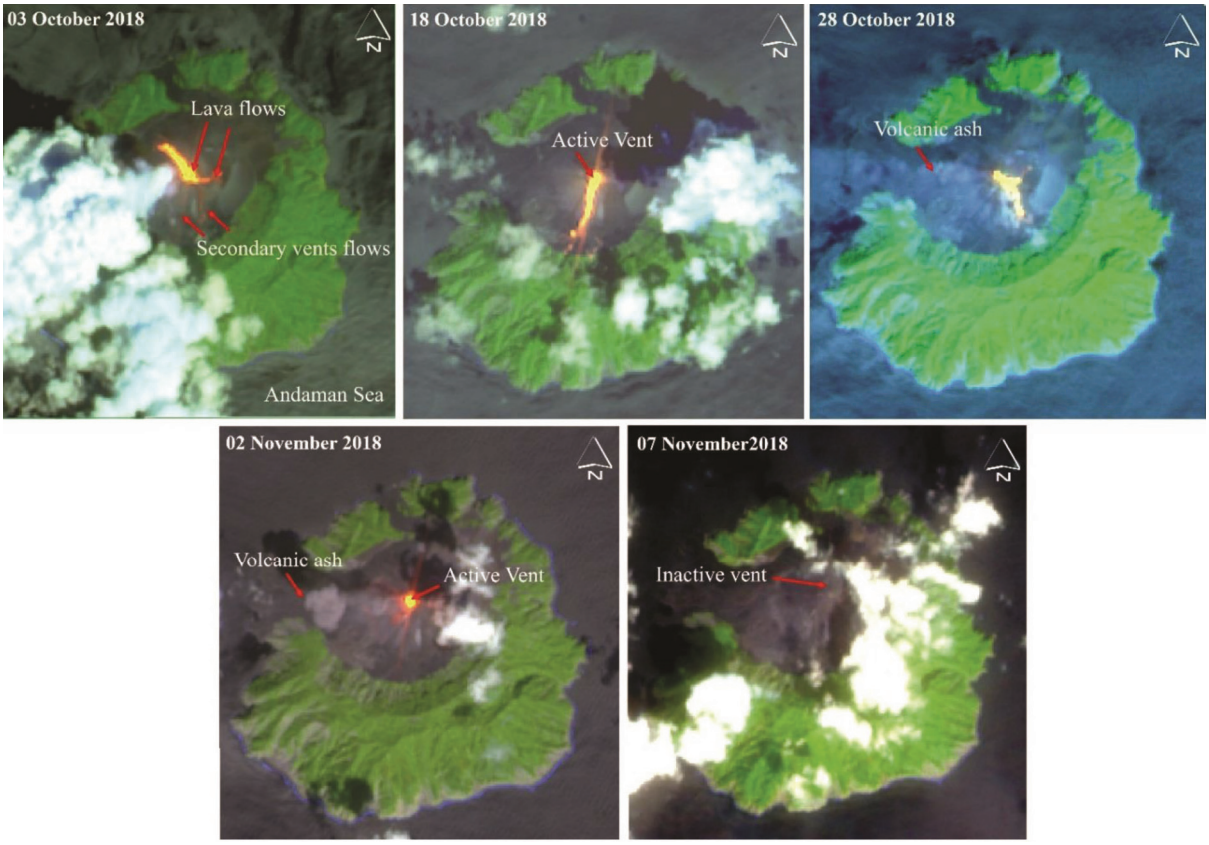

Figure 3. False colour composite images obtained from satellite images for the BIV using Arc GIS 10.1 software (https://www.esri.com/) (RGB = SWIR2:SWIR1: Red). Orange colour denotes current lava flow from the vent and black colour represents volcanic deposits.

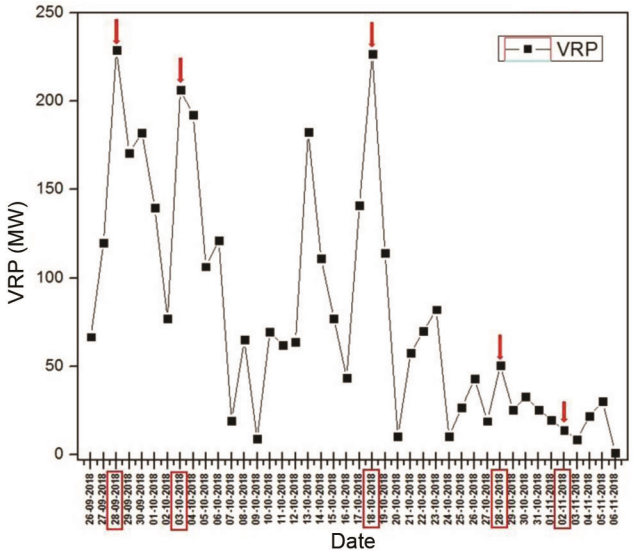

Figure 4. Time series of volcanic radiative power (VRP) recorded for BIV between 26 September 2018 to 6 November 2018. Red vectors and rectangle boxes indicate the active phase of the event corresponding to Figure 2. The data are plotted using origin Pro 8 SR4 (http://www.OrginLab.com).

eruptive phase of the volcano, whereas a decrease in heat flux is observed during the post eruption phase. Further, continuous variation in heat intensity during the 2018 eruptive phase can be noted. On 28 September 2018, the VRP values had increased (228.88 MW) compared to 27 June 2018 (120.05 MW). Similarly, on 3, 18 and 28 October 2018, VRP values (206.22, 22.66 and 50.70 MW respectively) had increased compared with prior activities on 2, 17 and 27 October 2018 (16.61, 14.11 and 19.11 MW respectively). On 2 November 2018, VRP had slightly decreased from 19.87 to 14.13 MW; this may be indicative of slowdown/fall in volcanic activity. The observed VRP values were also validated with Sentinel-2 images (Figure 3), which also shows a close relation with FIRMS thermal anomalies (Figure 5 *a*). The time series of VRP perfectly depict the active eruption phase of the volcano and also correspond with Sentinel-2 earth observatory satellite images and derived FIRMS datasets.

FIRMS and sulphur dioxide

Thermal anomaly was also observed in the form of anomalous fire pixels for 44 days, starting from 24 September 2018 to 6 November 2018 in the FIRMS database and was correlated with the latest volcanic eruptive activity (Figure 5 *a*). In the Sentinel-2 satellite images with FCC (RGB = SWIR2:SWIR1:Red), the glowing vent and lava flows in various directions could be observed during

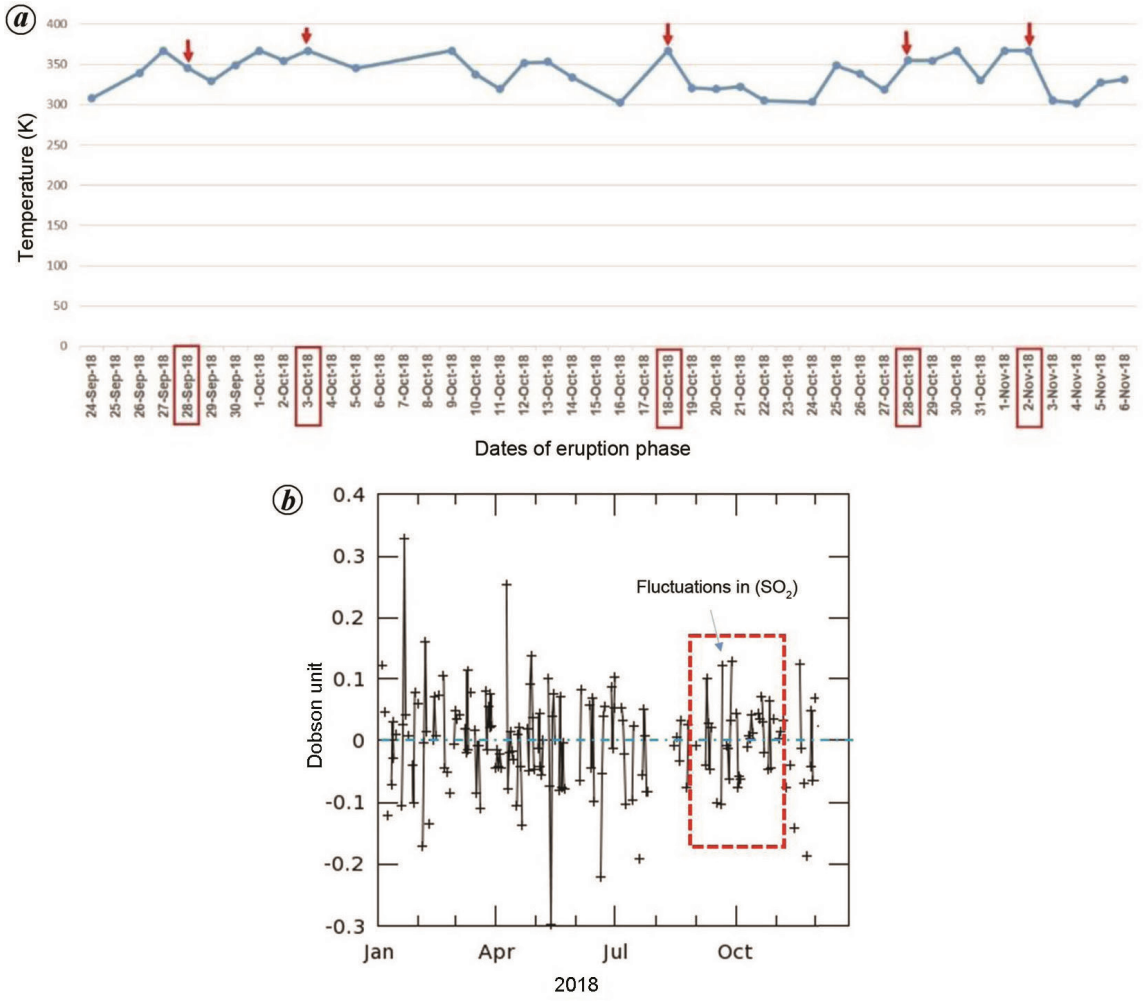

Figure 5. ***a***, Thermal anomalous from 24 September 2018 to 6 November 2018. Red colour box indicates the high temperature anomalies observed in the satellite images. ***b***, Sulphur dioxide (SO_2) fluctuations in 2018 for BIV. Red dashed box indicates sudden fluctuations in SO_2 from September to November 2018.

5 out of 44 fire days. The correlation for the remaining days could not be performed due to nonavailability of either cloud-free data or satellite pass. These data clearly show continuous thermal anomalous fluctuations and also complement the VRP during the study period (Figure 4).

In view of the 2018 active eruption phase, SO_2 data were analysed. As a result, sudden changes in SO_2 were observed during the 2018 eruption phase over BIV from September to November (Figure 5 *b*). The SO_2 observed was very low (≃0.1 to 0 DU) during pre-eruption. From mid-September to mid-November 2018, the SO_2 level started to fluctuate between 0 and 0.150 DU, which confirms the eruption activity and perfectly correlates with other optical and volcanic datasets used in the present study. As observed during the field study, this volcano had emitted ash/pyroclastic materials at an interval of 12–14 min (four times in an hour). The SO_2 data also help monitor and understand the behaviour of the remotely located volcanoes.

HYSPLIT modelling

In the present study, we have used a five-day forward trajectory and volcanic ash model for each eruption event which was estimated using the HYSPLIT model, to identify the transport pathways and extent of volcanic ash materials from BIV during the 2018 eruptive phase (from 25 September 2018 – till now) respectively. The five-day forward trajectories depict the transport of ash materials from the Barren Island for various major eruptive events in 2018 (Figure 6). In the present study, the altitudes of the trajectories were adopted at three different (above ground level) heights, viz. 500 m for within the atmospheric boundary layer, 1500 m for above the atmospheric boundary layer and 2500 m for the lower free troposphere. The analysis shows that in different eruptive phases, there are well demarcated, distinct transport paths of ash materials at individual altitudes. Most of pathways are dominated towards the west to northwest direction in

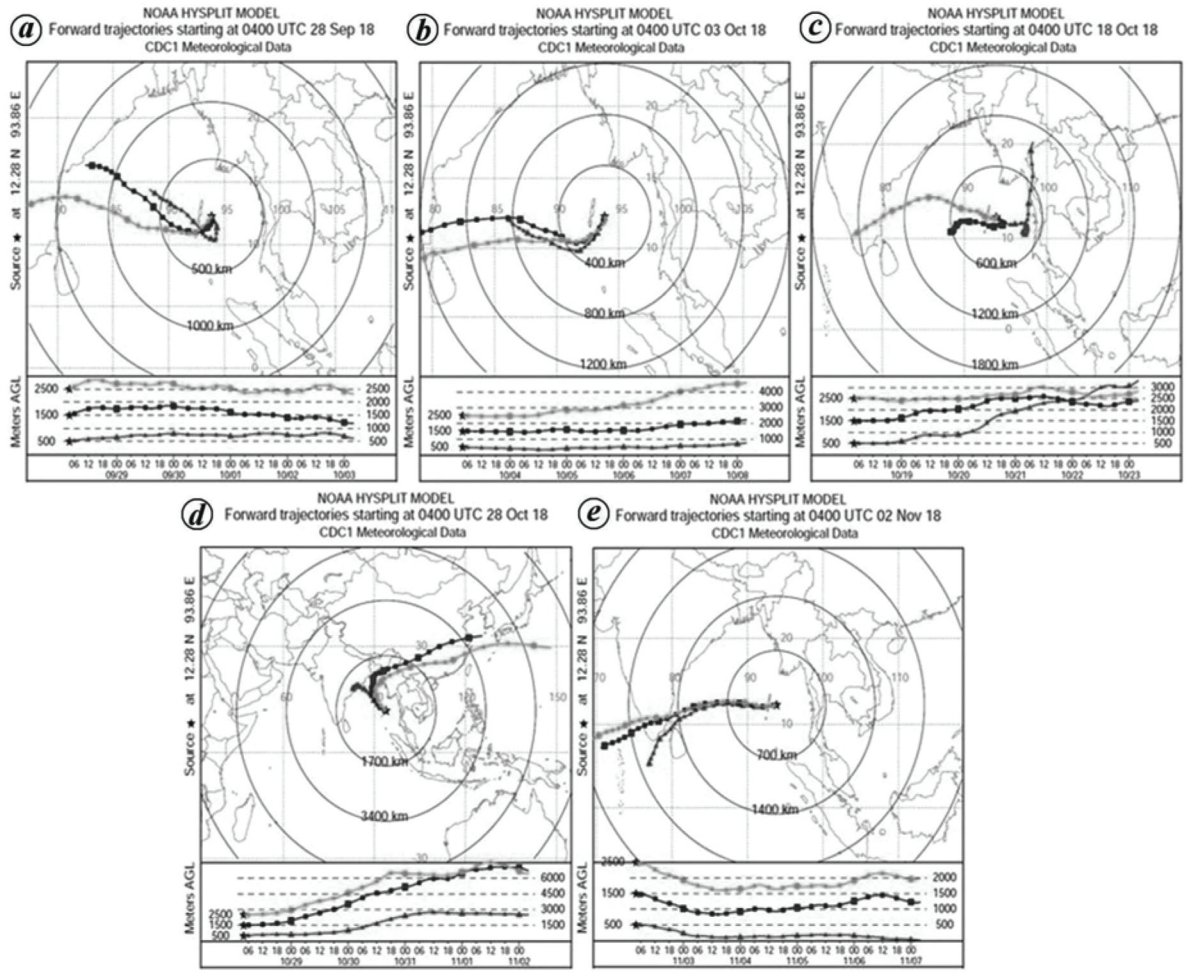

Figure 6. Transport pathways of volcanic ash calculated with HYSPLIT (https://www.ready.noaa.gov/HYSPLIT_traj.php). The plots are forward trajectory modelled using REANAYLSIS weather data for five days. Vertical velocities are taken from the weather model and do not include settling, and wind direction varies with altitude, but the map gives a general impression of wind direction. The start dates are (***a***) 28 September 2018, (***b***) 3 October 2018, (***c***) 18 October 2018, (***d***) 28 October 2018 and (***e***) 2 November 2018.

almost all distinct altitudes, which may affect the southern states of India like Tamil Nadu, Kerala and Andhra Pradesh along with neighbouring countries, viz. Sri Lanka. In an exceptional case (for example, the event of 28 October 2018 (Figure 6 *d*)), it initially dominated towards the northwest direction and curved towards northeast direction. The resultant ash may have affected the eastern neighbouring countries like Bangladesh, Thailand, Myanmar and China. However, the transport pathways of HYSPLIT model show that this volcano may not only affect the Indian states, but also the neighbouring countries.

Consequently, volcanic ash modelling has been carried out to identify the extent of ash cloud in the lower atmosphere (Figure 7). This model has been processed using the following run-time parameters, viz. summit elevation 1158 ft (352.95 m; USGS-assigned eruption source parameter), 24 h eruption duration and 48 h run time (eruption plus 48 h). The altitude of the present model varies from 200 to 550 m from summit elevation and the extent of volcanic ash area varies from metres to several kilometres (not measurable due to data limitations). In the final results, we observed similar trends in volcanic ash transport but not in the extension of volcanic materials. On 28 September 2018, the spread of ash cloud (represented in pink colour in Figure 7 *a*) was low and partially covered the Andaman Islands. With increase in run time, the spread of ash cloud also increased over the Andaman Islands and reached the Little Andaman Island, whereas VRP was high (228.88 MW) on the same day. Similarly, on 3 October 2018, initially the ash cloud spread was low and increased with run time, which covered the Andaman Islands (Figure 7 *b*). VRP was 206.22 MW on the same day. On 18 October 2018, the ash cloud spread was moderate and horizontal, showing tremendous increase with increase in run time, and covering the entire Andaman Islands in the east, reaching up to South Myanmar in the west (Figure 7 *c*). Whereas VRP on the same day was

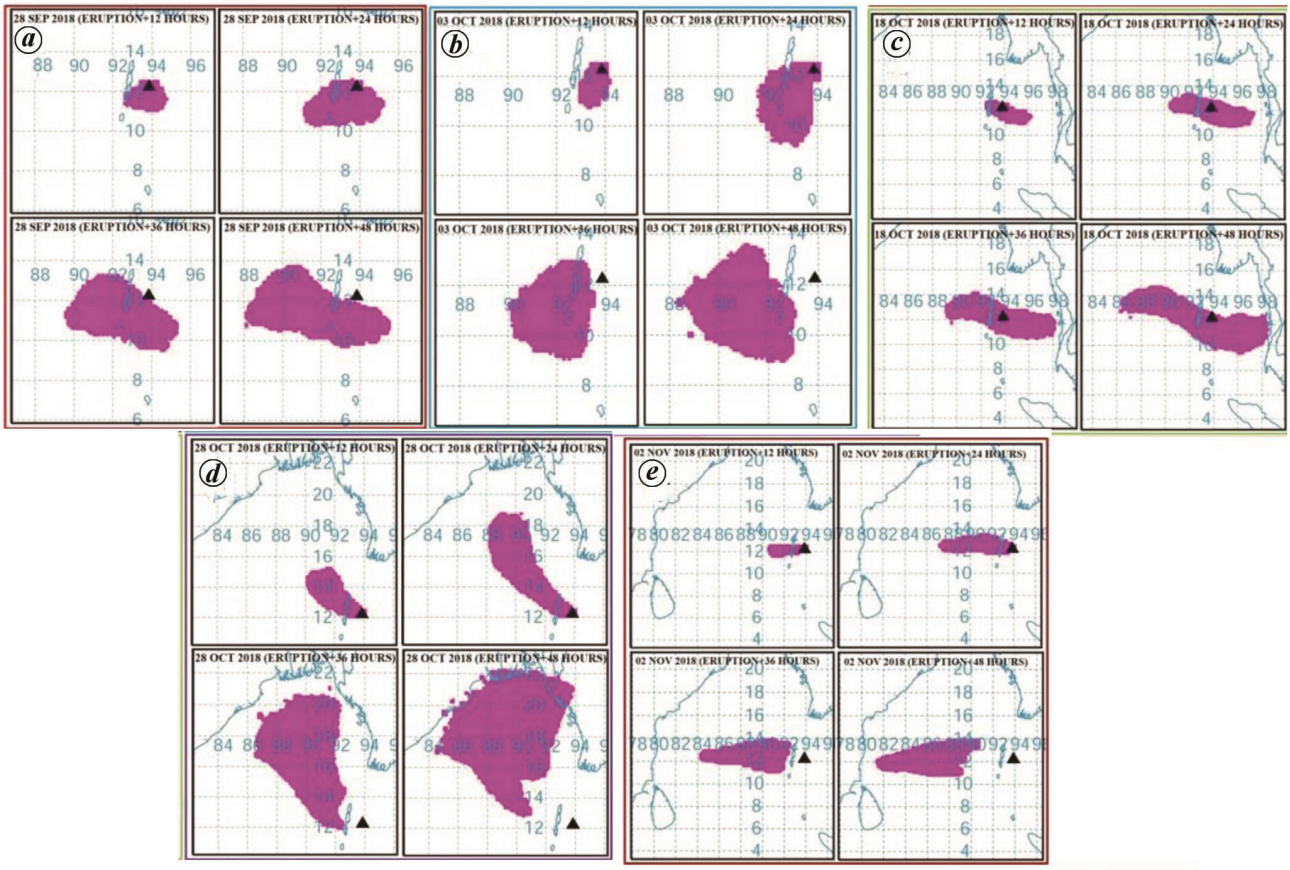

Figure 7. Volcanic ash model of BIV during the 2018 eruptive phase, modelled by HYSPLIT volcanic ash model: (***a***) 28 September 2018, (***b***) 3 October 2018, (***c***) 18 October 2018, (***d***) 28 October 2018 and (***e***) 2 October 2018 with 48 h run time.

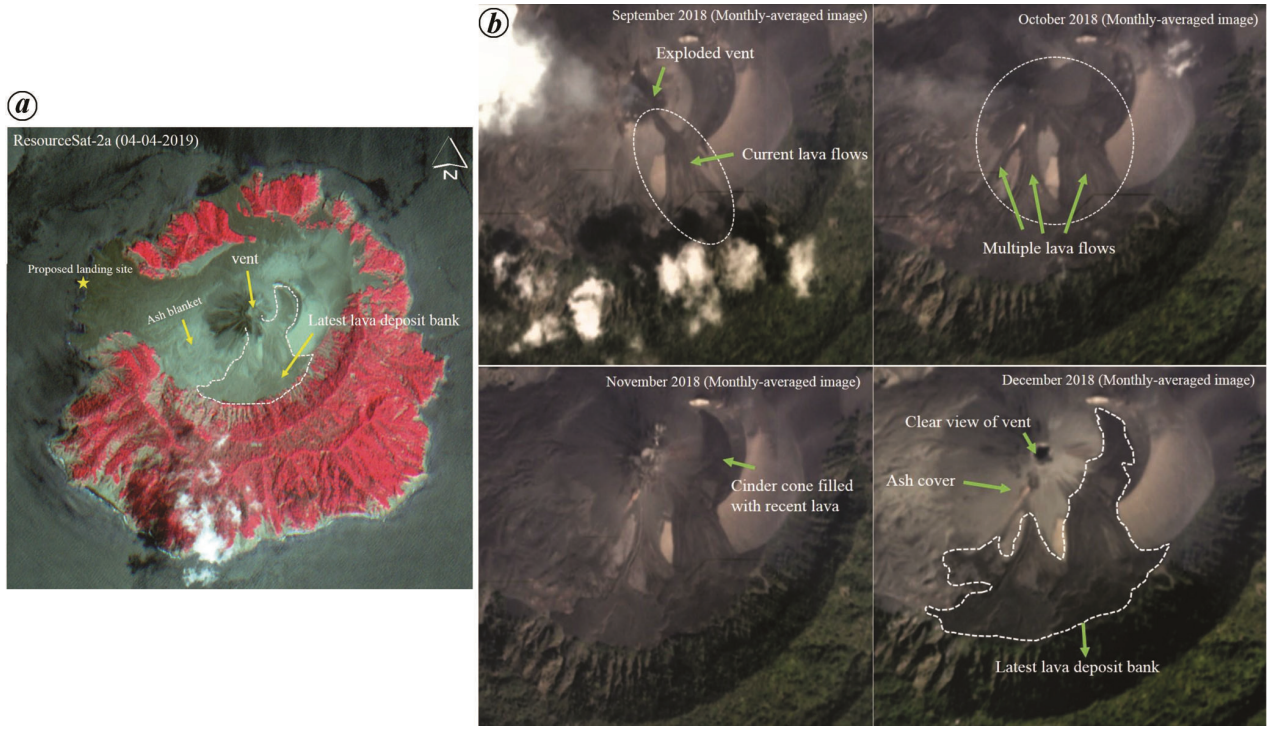

Figure 8. ***a***, ResourceSat-2 (NRSC) image of BIV of 4 April 2019. This image reveals various volcanic features, viz. latest lava flow (white polygon), vent and ash blanket. Yellow star represents the proposed landing site for field work. ***b***, High-resolution satellite image **(**Planet Explorer) snapshots of BIV from September 2018 to December 2018. These images demarcated of the latest 2018 eruptive phase lava flows, depositions and vent.

Figure 9. Volcanic gases entering the atmosphere in the active phase of the BIV in October 2018, during a period of sustained strombolian activity.

22.33 MW. Similarly, on 28 October 2018, the volcanic ash cloud was high and dynamically spread with run time (Figure 7 *d*). At the end of 48 h run time, ash clouds reached the eastern Indian states and the neighbouring countries of Bangladesh and Myanmar, whereas VRP was low (50.70 MW) on the same day. On 2 November 2018, the ash cloud spread was initially low and reached moderate stage after 48 h run time, and travelled towards the west. The ash cloud spread was high during low VRP values, as the high and low radiative values correspond to hot active eruptions and relatively cold gaseous emanations respectively[8].

Conclusion

We have analysed BIV during the 2018 active phase by combining various datasets, viz. Sentinel-2, MODIS–MIROVA (VRP), FIRMS (NASA/NOAA mission) and HYSPLIT together with field observations. During the end of 2018 and early 2019, two months of active volcanism was observed with several lava flows from the primary as well as secondary vents that have erupted forming fresh volcanic landforms (Figure 8 *a* and *b*). The current band combinations involving IR bands of Sentinel-2 (ESA) and Indian satellites (ISRO) have revealed the glowing vent and flow pattern along with formation of new volcanic landforms (lava flows). As observed previously, the direction of lava flow was towards the north due to presence of vent. With time, the vent had shifted and lava flows were also actively shifting towards south but in a few cases it was observed that the flows had travelled southwest. In the current situation, the active vent and lava flows are in the southern direction.

The analysed VRP time series showed the increasing thermal emissions ranging between 1 and 228 MW, with an overall average of 67.30 MW. The VRP results clearly depict the changes from low to high thermal regimes that indicate switching from open vent to effusive activity of BIV, similar to those observed for the Stromboli volcano in Italy. Further, the FIRMS thermal anomalies are also closely corresponded with periods of high eruptions as observed in the VRP and Sentinel-2 datasets. When compared with the conventional field-based observations (Figure 9), this integrated approach utilizing high-resolution datasets, VRP, FIRMS and OMI along with HYSPLIT has proven as an effective methodology in the continuous monitoring of active volcanoes, especially in inaccessible areas.

Conflicts of interest: The authors declare no competing interests.

1. Sheth, H. C., Ray, J. S., Kumar, A., Bhutani, R. and Awasthi, N., Toothpaste lava from the Barren Island volcano (Andaman Sea). *J. Volcanol. Geotherm. Res.*, 2001, **202**, 73–82.
2. Sheth, H., What drives centuries-long polygenetic scoria cone activity at Barren Island volcano? *J. Volcanol. Geotherm. Res.*, 2014 **289**, 64–80; https://doi.org/10.1016/j.jvolcanol.2014.10 .019.
3. Furtney, M. A., Synthesizing multi-sensor, multi-satellite, multi-decadal data sets for global volcano monitoring. *J. Volcanol. Geotherm. Res*., 2018 **365**, 38–56; https://doi.org/10.1016/j.jvolgeores.2018.10.002.
4. Campion, R., New lava lake at Nyamuragira volcano revealed by combined ASTER and OMI SO_2 measurements. *Geophys. Res. Lett*., 2014, **41**(21), 7485–7492; https://doi.org/10.1002/2014GL061808.
5. Ramsey, M. and Harris, A., Volcanology 2020: how will thermal remote sensing of volcanic surface activity evolve over the next decade? *J. Volcanol. Geotherm. Res.*, 2013, **249**, 217–233.

6. Harris, A. J. L., *Thermal Remote Sensing of Active Volcanoes. A User's Manual*, Cambridge University Press, Cambridge, UK, 2013, p. 736.
7. Vinod Kumar, K., Martha, T. R. and Roy, P. S., Detection of volcanic eruption in Barren Island using IRS P6 AWiFS data. *Curr. Sci*., 2016, **91**(6), 752–753.
8. Coppola, D., Thermal remote sensing for global volcano monitoring: experiences from the MIROVA system. *Front. Earth Sci*., 2020, **7**, 362.
9. Coppola, D., Laiolo, M., Cigolini, C., Delle Donne, D. and Ripepe, M., Enhanced volcanic hot-spot detection using MODIS IR data: results from the MIROVA system. *Geol. Soc. London*, *Spec. Publ.*, 2016, **426**(1), 181–205; https:/doi.org/10.1144/SP426.5.
10. Coppola, D., Laiolo, M., Lara, L. E., Cigolini, C. and OroZco, G., The 2008 'silent' eruption of Nevados de chillan (Chile) detected from space: effusive rates and trends from the MIROVA system. *J. Volcanol. Geotherm. Res*., 2016, **327**, 322–329; http://doi.org/10.1016/j.jvolgeo res.2016 .08.016.
11. Coppola, D. and Cigolini, C., Thermal regimes and effusive trends at Nyamuragira volcano (DRC) from MODIS infrared data. *Bull. Volcanol*., 2013, **75**, 744; https://doi.org/10.1007/s00445-013-0744-z.
12. Pieri, D. and Abrams, M., ASTER observations of thermal anomalies preceding the April 2003 eruption of Chikurachki volcano, Kurile Islands, Russia. *Remote Sensing Environ*., 2005, **99**(1–2), 84–94; doi.org/10.1016/j.rse.2005.06.012.
13. Blackett, M., Early analysis of landsat-8 thermal infrared sensor imagery of volcanic activity. *Remote Sensing*, 2014, **6**, 2282–2295.
14. Wright, R., Flynn, L. P. and Harris, A. J., Evolution of lava flowfields at Mount Etna, 27–28 October 1999, observed by Landsat 7 ETM+. *Bull. Volcanol*., 2001 **63**(1), 1–7; doi.org/10.1007/s004450100124.
15. Massimetti, F., Volcanic hot-spot detection using SENTINEL-2: a comparison with MODIS–MIROVA thermal data series. *Remote Sensing*, 2020, **12**, 820.
16. Francesco, M., Genzano, N., Neri, M., Falconieri, A., Giuseppe, M. and Pergola, N., A multi-channel algorithm for mapping volcanic thermal anomalies by means of Sentinel-2 MSI and landsat-8 OLI data. *Remote Sensing*, 2019, **11**, 2876; https://doi.org/.10.3390/rs11232876.
17. Gunda, G. K. T., Champatiray, P. K., Mamta, C. and Prakash, C., Monitoring of volcanic eruption (Barren Island) using EO satellites. *Curr. Sci*., 2020, **118**, 1874–1876.
18. Martha Tapas, R., Priyomvinod, K. and Kumranchat, Lava flows and cinder cones at Barren Island volcano, India (2005–2017): a spatio-temporal analysis using satellite images. *Bull. Volcanol.*, 2018, **80**, 15.
19. Bhattacharya, A., Reddy, C. S. S. and Srivastav, S K., Remote sensing for active volcano monitoring in Barren Island, India. *Photogramm. Eng. Remote Sensing*, 1993, **59**(8), 1293–1297.
20. Mitchell, A. H. G., Collision-related fore-arc and back-arc evolution of the northern Sunda Arc. *Tectonophysics*, 1985, **116**(3–4), 323–334.
21. Halder, D., Laskar, T., Bandopadhyay, P. C., Sarkar, N. K. and Biswas, J. K., Volcanic eruption of the Barren Island volcano, Andaman Sea. *J. Geol. Soc. India*, 1992, **39**, 411–419.
22. Sachin, T. *et al.* Morphology of submarine volcanic seamounts from inner volcanic arc of Andaman Sea. *Indian J. Geosci.*, 2018, **71**(3), 451–470.
23. Bandopadhyay, P. C., Inner-arc volcanism: Barren and Narcondam Islands. *Geol Soc., London, Memoirs*, 2017, **47**, 167–192.
24. Curray, J. R., The Sunda Arc: a model for oblique plate convergence. *Netherl. J. Sea Res*., 1989, **24**(2–3), 131–140.
25. Curray, J. R., Moore, D. G., Lawver, L. A., Emmel, F. J., Raitt, R. W., Henry, M. and Kieckhefer, R., Tectonics of the Andaman Sea and Burma: convergent margins. *Am. Assoc. Petrol. Geol. Mem.*, 1979, **29**, 189–198.
26. Curray, J. R., Tectonics and history of Andaman Sea region. *J. Asian Earth Sci*., 2005, **25**(1), 187–232.
27. Raju, K. A., Ramprasad, T., Rao, P. S. and Varghese, J., New insights into the tectonic evolution of the Andaman Basin, northeast Indian Ocean. *Earth Planet. Sci. Lett*., 2004, **221**(1–4), 145–162.
28. Wright, R., Flynn, L., Garbeil, H., Harris, A. and Pilger, E., Automated volcanic eruption detection using MODIS. *Remote Sensing Environ*., 2002, **82**(1), 135–155.
29. Rothery, D. A., Coppola, D. and Saunders, C., Analysis of volcanic activity patterns using MODIS thermal alerts. *Bull. Volcanol.*, 2005, **67**(6), 539–556; https://doi.org/10.1007/s00445-004-0393-3.
30. Wright, R., Flynn, L. P., Garbeil, H., Harris, A. J. L. and Pilger, E., MODVOLC: near-real-time thermal monitoring of global volcanism. *J. Volcanol. Geotherm. Res*., 2004, **135**, 29–49; https://doi.org/10.1016/j.jvolgeores.2003.12.008.
31. Wooster, M. J., Zhukov, B. and Oertel, D., Fire radiative energy for quantitative study of biomass burning: derivation from the BIRD experimental satellite and comparison to MODIS fire products. *Remote Sensing Environ*., 2003, **86**, 83–107.
32. Stein, A. F., Draxler, R. R., Rolph, G. D., Stunder, B. J. B., Cohen, M. D. and Ngan, F., NOAA's HYSPLIT atmospheric transport and dispersion modeling system. *Bull. Am. Meteorol. Soc.*, 2015, **96**, 2059–2077; doi:10.1175/BAMS-D-14-00110.1.
33. Draxler, R. R. and Hess, G. D., An overview of the HYSPLIT_4 modeling system for trajectories, dispersion, and deposition. *Aust. Meteorol. Mag.*, 1998, **47**, 195–308.
34. Draxler, R. R. and Hess, G. D., Description of the HYSPLIT_4 modeling system. NOAA tech. memo. ERL ARL-224. Air Resources Laboratory, Silver Spring, MD, pp 24, NTIS. PB98-116593.
35. Dare, R. A., Sedimentation of volcanic ash in the HYSPLIT dispersion model, CAWCR Technical Report No. 079, The Centre for Australian Weather and Climate Research, Melbourne, Australia, 2015.
36. Stunder, B., Heffter, J. L. and Draxler, R. R., Airborne volcanic ash forecast area reliability. *Weather Forecast.*, 2007, **22**, 1132, doi:10.1175/WAF1042.1.
37. Rolph, G. D. and Draxler, R. R., Description and verification of the NOAA smoke forecasting system: the 2007 fire season. *Weather Forecast.*, 2009, **24**, 361–378.
38. Draxler, R. R. and Rolph, G. D., Evaluation of the transfer coefficient matrix (TCM) approach to model the atmospheric radionuclide air concentrations from Fukushima. *J. Geophys. Res.*, 2012, **117**, D05107; doi:10.1029/2011JD017205.
39. Hurst, T. and Davis, C., Forecasting volcanic ash deposition using HYSPLIT. *J. Appl. Volcanol.*, 2017, **6**(5); doi:10.1186/s13617-017-0056-7.
40. Crawford, A. M., Stunder, B. J. B., Ngan, F. and Pavolonis, M. J., Initializing HYSPLIT with satellite observations of volcanic ash: a case study of the 2008 Kasatochi eruption. *J. Geophys. Res.: Atmos.*, 2016, **121**, 10786–10803; doi:10.1002/2016JD024779.

ACKNOWLEDGEMENTS. We thank the Department of Science and Technology, Government of India for providing the INSPIRE Fellowship (DST/INSPIRE Fellowship/2018/IF180050) to carry out this work. We thank Diego Coppola and his team for providing the VRP values and valuable inputs and suggestions; the Indian Coast Guard for ferrying us to the Barren Island; Chairman, ISRO for institutional support and the Department of Disaster Management, Pondicherry University, Port Blair for providing information and previous images they captured during the 2018 eruption phase.

Received 11 February 2021; revised accepted 2 April 2021

doi: 10.18520/cs/v121/i4/529-538